Powder Technology 319 (2017) 434–444

Contents lists available at ScienceDirect

Powder Technology

journal homepage: www.elsevier.com/locate/powtec

# A non-sampling mixing index for multicomponent mixtures

Migyung Cho [a], Prashanta Dutta [b], Jaesool Shim [c,*]

[a] Dept. of Game Engineering, Tongmyong University, Republic of Korea
[b] School of Mechanical and Materials Engineering, Washington State University, United States
[c] School of Mechanical Engineering, Yeungnam University, Republic of Korea

ARTICLE INFO

*Article history:*
Received 19 January 2017
Received in revised form 29 April 2017
Accepted 3 July 2017
Available online 05 July 2017

*Keywords:*
Non-sampling
Mixing index
Random mixing
Multicomponent mixtures
Powder

ABSTRACT

Uniform mixing is crucial for different types of molecules, powders, and materials in several chemical, mineral, cement, and drug companies. However, there is no effective index to evaluate the uniformity of mixing of multiple components. This study proposes a non-sampling mixing index (SMI) that is applicable to both multiple mixtures with more than two components as well as binary mixtures. The proposed mixing index estimates a mixing state by using all subdomain mixing information for all particles without requiring sampling. In the study, the index was used to predict the mixing of different types of metallic particles in a screw blender. A discrete element based numerical technique was used to determine the transient location of particles in a screw blender at different rotation rates. The effectiveness of the SMI was demonstrated by comparing it with other representative mixing indices. The effectiveness was elucidated using a model of a binary system in which two groups of particles were mixed from 0% (no mixing) to 100% (perfect mixing). The SMI indicated a linear correlation from 0 to near 1 between test mixing conditions and the mixing indices in contrast to other conventional methods that over-predicted the mixing conditions. With respect to the DEM simulation, the SMI displayed values between SMI = 0 at the initial stage and SMI = 0.9–0.94 at a fully random mixed condition for the rpm ranges corresponding to 15, 30, 45 and 60. The results also indicated that the SMI value of zero occurred at the boundaries with the exception of the bottom and that a considerably lower mixing index was obtained at boundaries as opposed to inner subdomains with respect to the fully random mixed condition ($t = 20$ s and rpm = 30).


## 1. Introduction

In various industries, such as food [1], drug [2], chemical [3] and cement industries [4,5], perfect mixing is essential as there are different types of particles that have different sizes and characteristics. Dough preparation in the food industry requires homogeneous mixing of flour particles (73% carbohydrate, 10% protein, and 2% fat), yeast, sugar, and salt [6]. Typically, single and twin-screw mixers are used to obtain better mixing quality [7]. In the pharmaceutical industry, small quantities of active pharmaceutical ingredients are blended with large amounts of excipients for a pharmaceutical dosage [8]. Content uniformity in drugs is very important to ensure safety and efficacy [9,10]. Inefficient blending can lead to increased variability in active components in the final dosage form, and this potentially threatens patient health [11].

In chemical and process industries, a variety of mixers including tumbler mixers, convective mixtures, high shear mixtures, hopper mixers, ribbon mixers, screw mixers and plowshare mixers are used to mix solid particles of different sizes, shapes and densities to achieve proper characteristics [12–17]. Uniform mixing of cement, soil and water is very important in the construction industry to obtain multicomponent building blocks [4,18] because the strength of a block depends on the composition of ingredients. Similarly, the performance of an asphalt pavement requires uniform mixing of multi-phase composite materials such as asphalt, cement binder, coarse and fine aggregates, and mineral fillers [19].

Computer simulations are widely used to examine the homogeneity of mixtures and to improve the design of mixers for better amalgamation. A mixing index is required to evaluate mixing conditions. Generally, the value of a mixing index should be between 0 and 1 wherein 0 implies no mixing of individual components (complete segregation) and 1 implies perfect mixing. A mixing index is used to determine optimized mixing in a specific system and it is important in identifying the design conditions of a mixer. For example, the incorrect indication of a high mixing index in a scenario involving poor mixing could lead to an incorrect decision that could result in the loss of a whole product batch. Therefore, it is very important to accurately determine the mixing index.

There are various types of mixing indices that are primarily classified into two categories. The first category is based on statistical analysis using standard deviation from spot samplings [20–23] while the other category uses all particles in a system as opposed to a few particles from samplings [24–26]. Statistical mixing indices involve critical disadvantages such as variation with sampling size and sampling conditions [27]. Specifically, it is necessary for all particles to possess a

* Corresponding author.
*E-mail address:* jshim@ynu.ac.kr (J. Shim).

http://dx.doi.org/10.1016/j.powtec.2017.07.011
0032-5910/

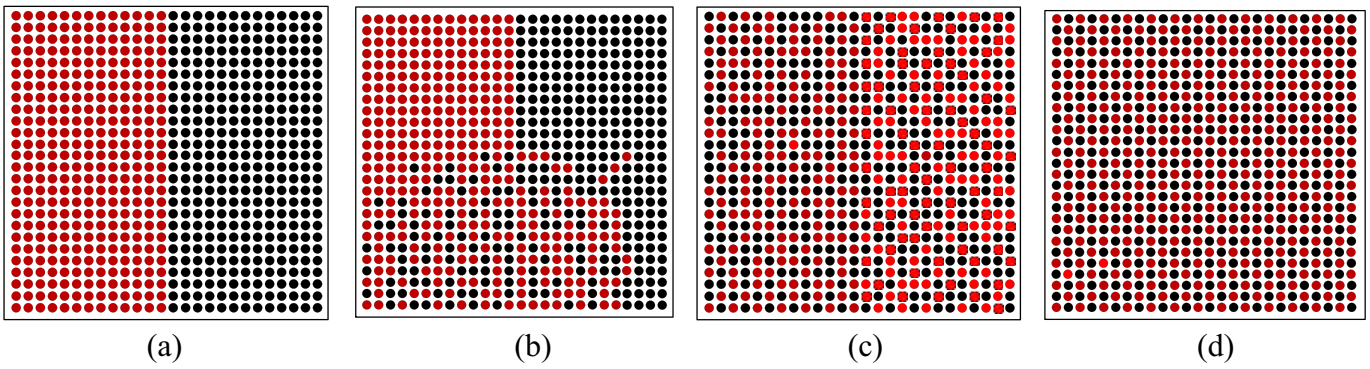


**Fig. 1.** A schematic of mixing stages: (a) completely segregated, (b) partially mixed, (c) fully random mixed, and (d) perfectly mixed.

uniform size in the case of the Lacey index. The generalized mean mixing index (GMMI) uses the contribution of all particles in calculating the index [24] although the GMMI routinely over-predicts the mixing (with a mixing index higher than 1) and does not provide a single index for a mixture. Subsequently, the modified generalized mean mixing index (MGMMI) [25] was introduced to bind a mixing index between 0 and 1. However, the disadvantage of the MGMMI involves overestimating the mixing state such that it results in a value close to 1 even if mixtures are segregated.

The present study focuses on resolving existing issues in extant mixing indices by presenting a new mixing index based on subdomain analysis. The proposed method uses all particles to evaluate the mixing condition and therefore constitutes a non-sampling mixing index. The advantage of the proposed index is that it provides a linear correlation between the mixing condition of mixtures and the mixing index that is close to 0 when mixing does not occur and close to 1 when near perfect mixing occurs. In the study, the effectiveness of the index SMI was demonstrated for several model systems.

The rest of the paper is organized as follows. Section 2 discusses the advantages and disadvantages of conventional mixing indices. This is followed by introducing the mathematical basis for the proposed index. Both binary and ternary model systems are presented to demonstrate the efficacy of the proposed index when compared with other methods. This is followed by examining a mathematical model and simulation tool for a discrete element method (DEM) that is used to obtain particle mixing in a screw blender. Finally, conclusions of our study are presented.

## 2. Conventional mixing indices

Computer simulations are widely used to design different types of mixers. These simulation tools can provide both spatial and temporal information for all particles in the computational domain. This information is readily available in a computer simulation, and thus it is desirable to obtain a method based on the locations of all particles. This section briefly discusses existing mixing indices and compares them with the proposed index.

Although perfect mixing is desirable in several processes, it is unachievable due to the tendency of particles to segregate, diffuse and display convection. Segregation occurs when a system contains particles with different sizes or densities or when selective forces are applied [28]. However, diffusion and convection prevent particles from segregating. Hence, conditions between perfect segregation and perfect mixing are obtained in actual mixing operations. Fig. 1(a)–(d) shows four different stages that may be encountered in a mixing operation. A perfectly mixed condition is rarely achieved in mixing operations. Instead, a fully random mixing state is highly likely to occur in an equilibrium mixing state owing to particle diffusion and segregation.

### 2.1. Mixing indices based on statistics

A variety of mixing indices were developed to essentially evaluate the quality of a mixture in field industries that require uniform mixing of two or more types of molecules with respect to their products. Most mixing indices in the literature were developed for binary mixtures and based

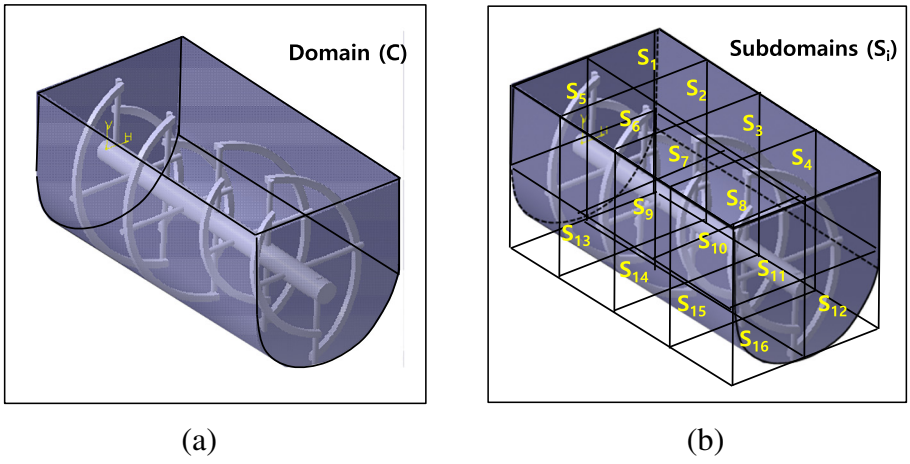


**Fig. 2.** A schematic of the mixing domain. (a) Entire mixing domain C prior to sectioning (b) subdomains to estimate the mixing index. $n_w = 4$, $n_h = 2$, and $n_d = 2$. Subdomains are treated in a manner similar to three-dimensional grid elements used in the finite volume or finite element method.

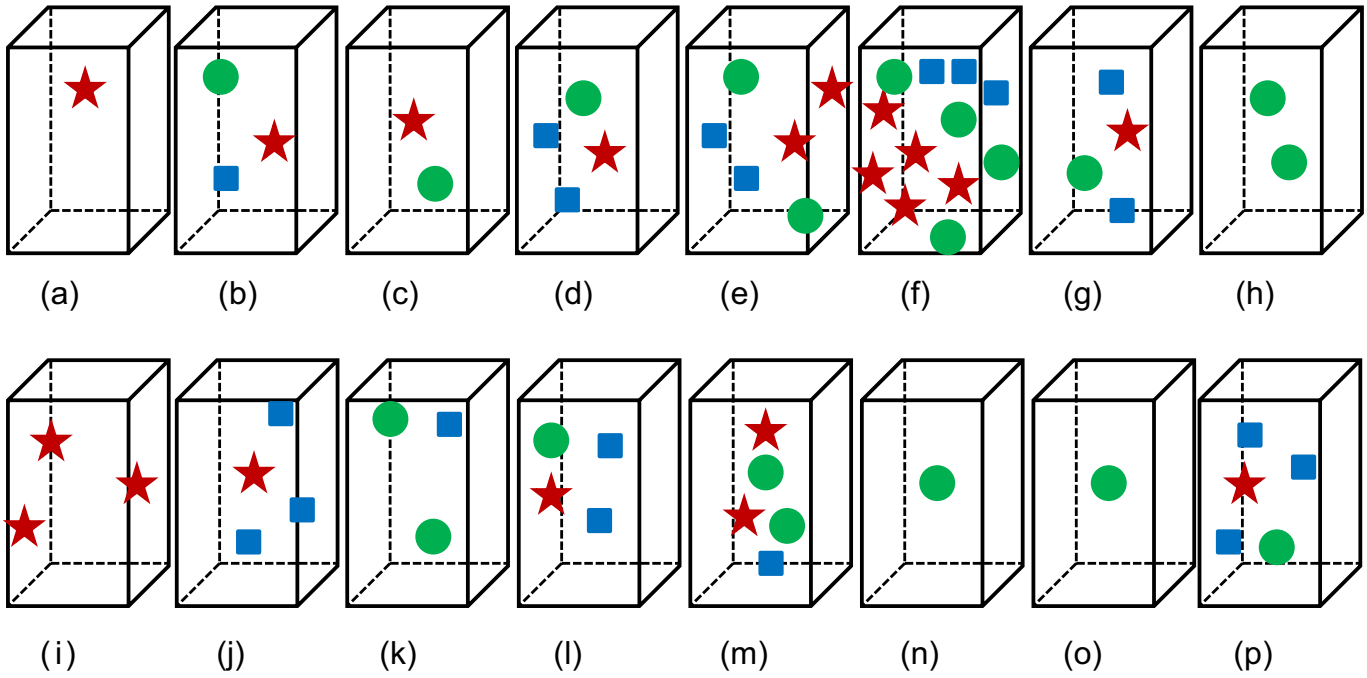


**Fig. 3.** Hypothetical particle distribution in all 16 subdomains (a–p) that are considered in Fig. 2 to estimate the overall mixing index based on subdomain mixing information. There are 20 particles for each category (red stars, green circles, and blue rectangles). (For interpretation of the references to color in this figure legend, the reader is referred to the web version of this article.)

on statistical analysis and specifically on standard deviation, variance and the coefficient of variation of the composition between samples drawn from a mixture [29,30]. Extant studies, including Lacey [21], Kramer [31] and Ashton and Valentin [32] proposed mixing indices based on statistics.

The Lacey index is a very frequently used mixing index that is based on the standard deviation for a binary mixture. The Lacey Index M that is based on the fraction of particles in a sample is defined as follows [21]:

$$M = \frac{S_0^2 - S^2}{S_0^2 - S_R^2} \tag{1}$$

In Eq. (1), $S_0^2$ represents the variance at the time when the components of the mixture are completely segregated, $S_R^2$ denotes the variance at the time when they are fully mixed, and $S^2$ is the variance for a mixture between fully random and completely segregated mixtures. In practice, Eq. (1) includes a statistical meaning as measured by considering a sufficiently high sampling dataset. The Lacey index suffers from an availability problem due to the size-dependence of the extracted sample and shows erroneous results when the geometrical size of the components of a mixture is not identical [22]. The main disadvantage of mixing indices based on standard deviation or variance is that they suffer from a lack of statistical accuracy in systems with an insufficient number of samples. Additionally, they vary with sampling size and sampling

**Table 1**
Estimation of the total mixing index from subdomain based mixing information for cases shown in Figs. 3 and 4.

| Total initial particle in domain C | Red star: 20 | | | Red star: 25 | | | Red star: 20 | Red star: 25 |
|---|---|---|---|---|---|---|---|---|
| | Green circle: 20 | | | Green circle: 20 | | | Green circle: 20 | Green circle: 20 |
| | Blue square: 20 | | | Blue square: 15 | | | Blue square: 20 | Blue square: 15 |
| Desired mixing ratio | 1:1:1 | | | 5:4:3 | | | 1:1:1 | 5:4:3 |
| Participation factor | | | | | | | $f_1 = 1, f_2 = 1, f_3 = 1$ | $f_1 = 1, f_2 = 1.25, f_3 = 1.67$ |
| | Red star | Green circle | Blue square | Red star | Green circle | Blue square | SMI ($S_i$) | SMI ($S_i$) |
| a | 1 | 0 | 0 | 1 | 0 | 0 | 0 | 0 |
| b | 1 | 1 | 1 | 1 | 1 | 1 | 1 | 0.675 |
| c | 1 | 1 | 0 | 1 | 1 | 0 | 0.5 | 0.4 |
| d | 1 | 1 | 2 | 1 | 1 | 2 | 0.5 | 0.3375 |
| e | 2 | 2 | 2 | 2 | 2 | 2 | 1 | 0.675 |
| f | 5 | 4 | 3 | 5 | 4 | 3 | 0.7 | 1 |
| g | 1 | 1 | 2 | 1 | 1 | 2 | 0.5 | 0.3375 |
| h | 0 | 2 | 0 | 0 | 2 | 0 | 0 | 0 |
| i | 3 | 0 | 0 | 3 | 0 | 0 | 0 | 0 |
| j | 1 | 0 | 3 | 1 | 0 | 2 | 0.167 | 0.15 |
| k | 0 | 2 | 1 | 0 | 1 | 1 | 0.25 | 0.375 |
| l | 1 | 1 | 2 | 1 | 2 | 1 | 0.5 | 0.5333 |
| m | 2 | 2 | 1 | 2 | 1 | 0 | 0.75 | 0.3125 |
| N | 0 | 1 | 0 | 2 | 1 | 0 | 0 | 0.3125 |
| o | 0 | 1 | 0 | 2 | 2 | 0 | 0 | 0.4 |
| p | 1 | 1 | 3 | 2 | 1 | 1 | 0.333 | 0.729 |
| SMI | | | | | | | 0.5206 | 0.5217 |

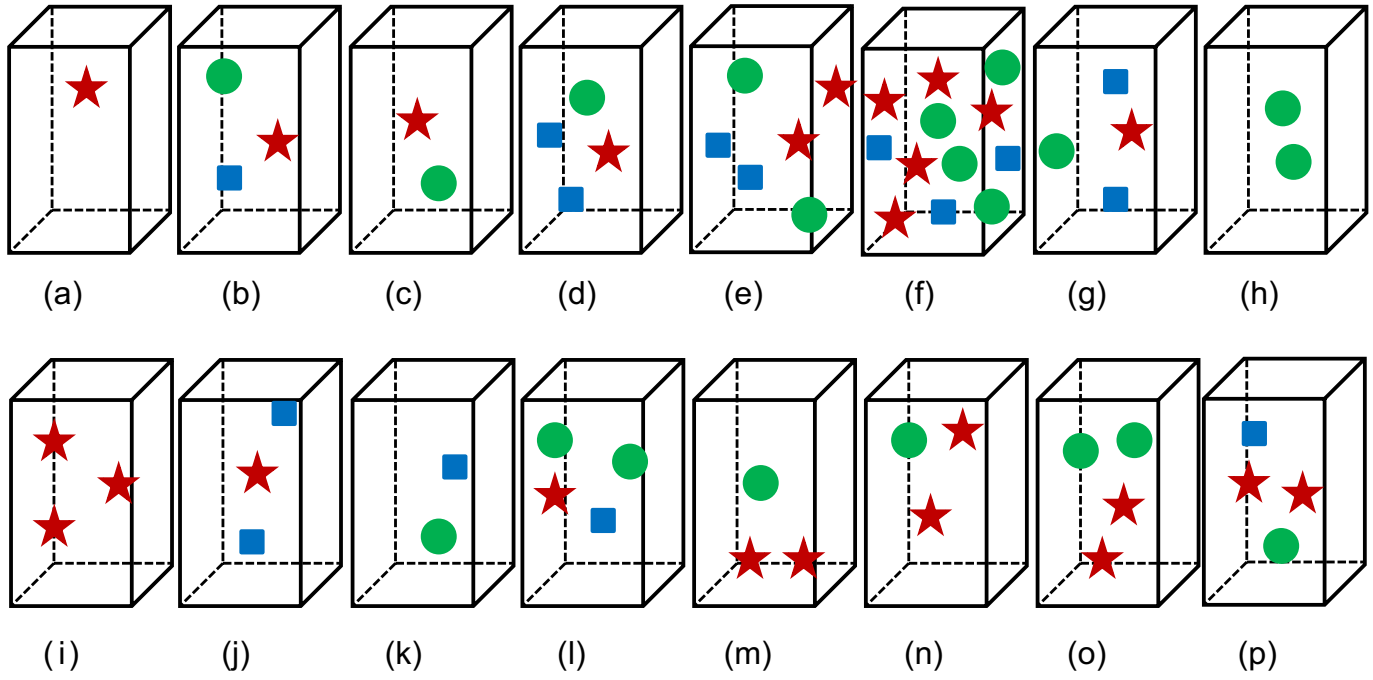


**Fig. 4.** Illustration of subdomain mixing index for different numbers of particles for each type of particle. (a)–(p) Hypothetical particle distribution in 16 subdomains considered in Fig. 2. There are 25 star, 20 circle, and 15 rectangle particles.

methods [27]. Hence, mixing indices based on statistics are subject to the fore-mentioned limitations.

### 2.2. Mixing indices with all particles

The GMMI corresponds to a very simple and fast method for evaluating mixing performance from the coordinates of all particles [24]. This is calculated for multicomponent mixtures irrespective of the number of particle types. The method is applied to all particles without a sampling process such that a meaningful mixing index can be obtained from even a small number of particles.

For a mixture composed of $Q$ types of particles and $N$ total number of particles, the GMMI is defined for particle type $k$ ($1 \le k \le Q$) as follows:

$$GMMI_k = \frac{GMMI_{xk} + GMMI_{yk} + GMMI_{zk}}{3} \tag{2}$$

$$GMMI_{xk} = \frac{\sum_{j=1}^{N_k}(x_j - x_{ref})/N_k}{\sum_{j=1}^{N}(x_j - x_{ref})/N}, \quad GMMI_{yk} = \frac{\sum_{j=1}^{N_k}\left(y_j - y_{ref}\right)/N_k}{\sum_{j=1}^{N}\left(y_j - y_{ref}\right)/N} \quad \text{and} \quad GMMI_{zk} = \frac{\sum_{j=1}^{N_k}(z_j - z_{ref})/N_k}{\sum_{j=1}^{N}(z_j - z_{ref})/N} \tag{3}$$

where $GMMI_{xk}$, $GMMI_{yk}$ and $GMMI_{zk}$ correspond to the generalized mean mixing indices in the $x$, $y$, and $z$ coordinates, respectively. Furthermore, $N_K$ denotes the number of $k$-type particles, and $x_{ref}$, $y_{ref}$, and $z_{ref}$ denote coordinates of an arbitrary reference point. Although this index offers a few advantages when compared with statistical methods, it can correspond to a value that exceeds 1, which is unrealistic. Additionally, the GMMI can also correspond to 1 even in the case of $GMMI_x < 1$, $GMMI_y < 1$ and $GMMI_z > 1$. A previous study by Siraj et al. [25] modified the GMMI scheme to avoid mixing indices that exceed 1 as follows:

$$MGMMI_k = 1 - \frac{|1 - GMMI_{xk}| + |1 - GMMI_{yk}| + |1 - GMMI_{zk}|}{3} \tag{4}$$

Both GMMI and MGMMI have advantages, including the ease of implementation, speed of evaluation and the lack of dependence on sample size. Nevertheless, they involve serious disadvantages because they are based on the mean position of particles. For example, both GMMI and MGMMI can provide a value close to 1 even when mixing is locally poor. The overestimated index can result in wrong information with respect to mixing conditions and thus this may correspond to an ideal index.

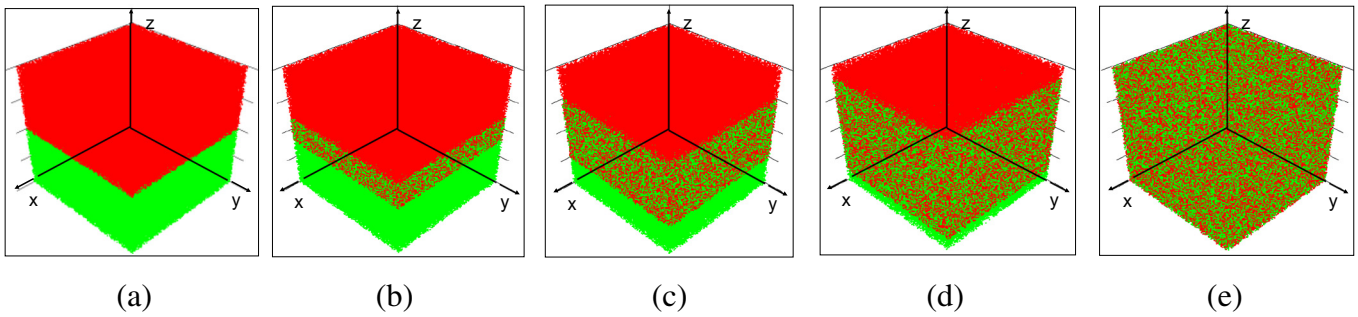


**Fig. 5.** Binary mixtures of 1,000,000 red and 1,000,000 green particles for (a) 0%, (b) 20%, (c) 50%, (d) 80%, and (e) 100% mixing. The radius of each particle corresponds to 1 mm with respect to the domain ($0 \le x, y, z \le 200$ mm). (For interpretation of the references to color in this figure legend, the reader is referred to the web version of this article.)

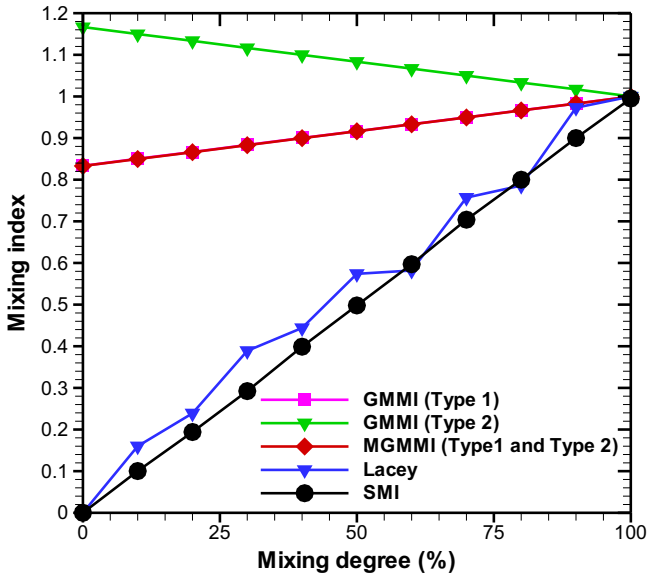


**Fig. 6.** Correlation test of various mixing indices.

## 3. Subdomain-based mixing index, SMI

The aim of the present study involves designing a new mixing index to satisfy the following five requirements. First, the mixing index should correspond to zero when the particle types are completely separated or segregated. Second, the mixing index should correspond to one when a mixture is perfectly mixed irrespective of $x$, $y$, or $z$ reference coordinates. Third, the mixing index should range between 0 and 1 and increase linearly with the degree of mixing. Fourth, the mixing index should be computed in the same manner for both a binary mixture as well as a multi-component mixture. Fifth, in the case of both binary and multi-component mixtures, a mixture should only correspond to a mixing index irrespective of the number of components.

The core idea of the proposed index involves obtaining local mixing information from all spatial elements known as subdomains and integrating them to determine the overall index. An arbitrary geometry for mixing $Q$ types of particles is considered as shown in Fig. 2(a). It is possible to fit any 3D object with an arbitrary shape into a rectangular prism with volume $V$ as shown in Fig. 2(b). The prism can be divided into several smaller subdomains by dividing the width, height, and depth by a specific number of elements.

If the prism is divided into $n_w$, $n_h$, and $n_d$ elements with respect to the width, height, and depth respectively, the total number of subdomains can be expressed as follows:

$$M = n_w \times n_h \times n_d \tag{5}$$

Fig. 2(b) shows 16 subdomains for an arbitrarily shaped screw blender where $n_w = 4$, $n_h = 2$, and $n_d = 2$. The subdomains can also correspond to different shapes based on the geometry of the mixer. With respect to $n_{ki}$ particles of type $k$ in the subdomain $S_i$, the number of all types of particles in $S_i$ corresponds to $\sum_{k=1}^{Q} n_{ki}$. Finally, the total number of particles ($N$) for the entire domain $V$ is as follows:

$$N = \sum_{i=1}^{M} \sum_{k=1}^{Q} n_{ki} \tag{6}$$

It is assumed that every type of particle initially possesses the same number of total particles. Thus, the fraction with respect to the highest value of the number of particles relative to other types of particles in subdomain $S_i$ is defined as follows:

$$P_{ki} = \frac{n_{ki}}{\max(n_{1i},\ n_{2i},\ n_{3i},\ \ldots n_{Qi})} \le 1, \quad 1 \le k \le Q \tag{7}$$

It should be noted that the quantity $P_{ki}$ does not actually correspond to the fraction of type "$k$" particles that typically represent a part of a whole. Two or more types of particles in a subdomain could possess the same maximum number of particles and in that case only one of these types of particles is selected to determine the denominator in Eq. (7). The subdomain mixing index for $S_i$ is simply obtained from the arithmetic mean of the individual fractions of each particle of type $k$ with the exception of the fraction of the majority type.

$$SMI(S_i) = \frac{1}{Q-1}\left(\sum_{k=1}^{Q} P_{ki} - 1\right) \tag{8}$$

The value of $SMI(S_i)$ corresponds to 1 only when each type of particle has the same number in the subdomain. The value corresponds to 0 when only one type of particle exists in the subdomain, thereby indicating complete segregation. If there are no particles in the subdomain, then the mixing index is not considered for that subdomain because the absence of all particles does not contribute to the SMI value. With respect to all other scenarios, the subdomain index corresponds to a value between 0 and 1.

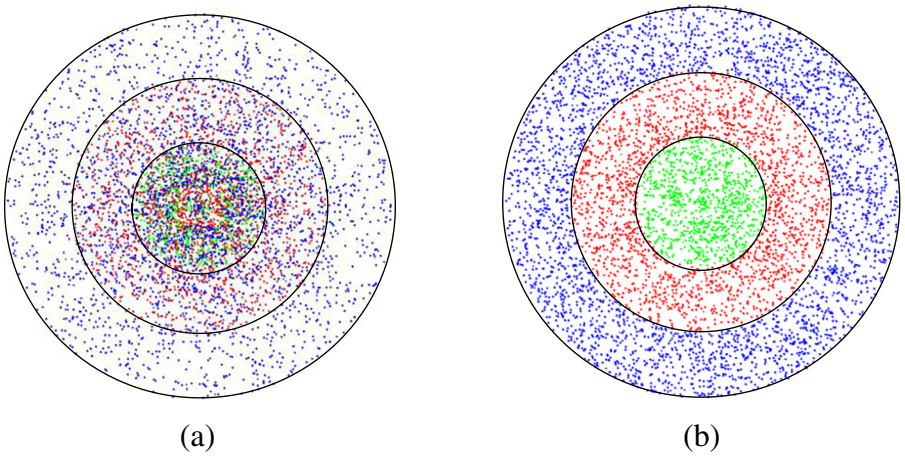


**Fig. 7.** A schematic view of mixing of three types of 2 mm particles (4000 particles of each type of particles). (a) Green is only present in the inner shell ($0 \le r_1 \le 200$ mm), red is present in the inner and middle shell ($0 \le r_2 \le 400$ mm) and blue is present in all three shells ($0 \le r_3 \le 600$ mm). (b) Green is only present in the inner shell, red is present in the middle shell and blue is present in the outer shell. (For interpretation of the references to color in this figure legend, the reader is referred to the web version of this article.)

Fig. 3(a)–(p) illustrate the particle distributions for all 16 subdomains as an example of each type with the same number of particles. Specifically, 20 particles were considered for each of the star, circle and rectangle types, and the desired mixing ratio is 1:1:1. The subdomain mixing index for each subdomain is shown in Table 1. For the particle distribution shown in Fig. 3(a)–(p), perfect mixing is obtained for Fig. 3(b) (1 star particle, 1 circle particle, and 1 rectangle particle) and Fig. 3(e) (2 star particles, 2 circle particles, and 2 rectangle particles) because the particle ratio is identical to the desired ratio. Conversely, no mixing is predicted for Fig. 3(a) (1 star particle), Fig. 3(h) (2 circle particles), Fig. 3(i) (3 rectangle particles), Fig. 3(n) (1 circle particle), and Fig. 3(o) (1 circle particle). These are examples of segregation because only a single type of particle is present.

The subdomain mixing index predicts 50% of the mixing for Fig. 3(c) (1 star particle and 1 circle particle), Fig. 3(d), (j), and (l) (1 star particle, 1 circle particle, and 2 rectangle particles). This mixing result can be justified easily from a physical point of view. For example, in Fig. 3(c), a star particle creates a perfect mixture if a circle particle and a rectangle particle are present. However, a rectangle particle does not exist in Fig. 3(c), and thus the mixing is only 50% effective in this subdomain. Similarly, in Fig. 3(d), two rectangle particles can create a perfect mixture with two star particles and two circle particles. Nevertheless, only a circle particle and a star particle are present, and thus the mixing is only 50% efficient. The second highest mixing is obtained in Fig. 3(m) (2 star particles, 2 circle particles, and 1 rectangle particle) due to the lack of a rectangle particle for perfect mixing.

### 3.1. Corrections for different particle ratios

If the initial particle count is different for each type of particle, then it is necessary to correct the index to handle the desired mixing ratio. If a system consists of $k$ types of particles ($1 \le k \le Q$) then the participation factor of particle type $k$ can be calculated as follows:

$$f_k = \frac{\max\left(\sum_{i=1}^{M} n_{1i},\ \sum_{i=1}^{M} n_{2i},\ \sum_{i=1}^{M} n_{3i},\ \ldots \sum_{i=1}^{M} n_{Qi}\right)}{\sum_{i=1}^{M} n_{ki}} \tag{9}$$

The fraction of particle type $k$ of Eq. (7) can be modified as follows:

$$P_{ki} = \frac{n_{ki} f_k}{\max\left((n_{1i} f_1),\ (n_{2i} f_2),\ (n_{3i} f_3),\ \ldots (n_{Qi} f_Q)\right)} \le 1, \quad 1 \le k \tag{10}$$

Thus, it is possible to determine the subdomain mixing index in this case by combining Eqs. (8) and (10).

In order to demonstrate this correction, a system consisting of three types of particles (25 star particles, 20 circle particles, and 15 rectangle particles) is considered as shown in Fig. 4(a)–(p). In this case, the desired mixing ratio corresponds to 5:4:3 based on the initial particle count. The particle distribution is exactly identical to that in Fig. 3(a)–(p) for the first nine subdomains of Fig. 4(a)–(i). The subdomain mixing index predicts perfect mixing for Fig. 4(f) (5 star particles, 4 circle particles and 3 rectangle particles) as shown in Table 1 as the particle ratio is identical to the desired mixing ratio.

In contrast, Fig. 4(b) and (e) do not have perfect mixing although they have the same numbers of star, circle, and rectangle particles. In a manner similar to the aforementioned case in Fig. 3(a)–(p) (1:1:1 desired mixing), the subdomain mixing index corresponds to 0 (no mixing) if only one type of particle is present in a subdomain. The examples shown in Figs. 3 and 4 confirm that the index can correspond to 0 (no mixing) to 1 (perfect mixing) in a subdomain for any type of desired mixing ratio irrespective of the number of different types of particles.

**Table 2**
A comparison of mixing indices for three-component mixtures. It should be noted that the Lacey index is not applicable for a multi-component system.

| Data | Color (type) | GMMI | MGMMI | SMI |
|---|---|---|---|---|
| Fig. 7(a) | Green | 0.9961 | 0.9961 | 0.3554 |
| | Red | 1.0009 | 0.9970 | |
| | Blue | 1.0030 | 0.9970 | |
| Fig. 7(b) | Green | 1.0006 | 0.9955 | 0 |
| | Red | 1.0023 | 0.9972 | |
| | Blue | 0.9970 | 0.9970 | |

### 3.2. Total mixing index

The total mixing index is computed from the subdomain mixing indices. With respect to M subdomains, the total mixing index is obtained by averaging each mixing index of all subdomains as follows:

$$SMI = \frac{1}{N} \sum_{i=1}^{M} \left[ SMI(S_i) \sum_{k=1}^{Q} (n_{ki}) \right] \tag{11}$$

The equation is averaged based on the number of particles in each subdomain. Thus, if the number of particles in a subdomain exceeds that in another subdomains, then the highly populated subdomain displays a greater contribution in the total mixing index. For example, both Fig. 3(b) and (e) result in a subdomain mixing index (SMI) of 1 because they possess the same numbers of each type of particles. However, the weightage of Fig. 3(e) is twice that of Fig. 3(b). The model predicts that the total mixing for the case in Fig. 3 corresponds to 0.5206 while that for Fig. 4 corresponds to 0.5217.

## 4. Comparison with other mixing indices

### 4.1. Model system for binary mixing

In order to test the linear relationship between the mixing condition and the mixing index, a binary system consisting of 2,000,000 particles in a 20-cm cube is considered in which the numbers of both type 1 as red and type 2 as green are the same. The mixing conditions between the red and green particles are artificially produced using a Mersenne Twister generator with the best known randomness. The mixing volume is precisely controlled as shown in Fig. 5(a)–(e). As shown in Fig. 5(a), the red and green particles are completely segregated, and the bottommost layer of red particles touches the topmost layer of green particles. Hence, the coordinates of green particles are generated in $0 \le x,z \le 200$ mm and $0 \le y \le 100$ mm while the coordinates of red particles are located in $0 \le x,z \le 200$ mm and $100 < y \le 200$ mm. As shown in Fig. 5(b), with respect to the location of 400,000 particles (200,000 red and 200,000 green), 20% of the total particles are in $0 \le x,z \le 200$ mm and $90 < y \le 110$ mm. The remaining 80% of the total particles, 800,000 green particles are in $0 \le x,z \le 200$ mm and $0 \le y \le 90$ mm while 800,000 red particles are in $0 \le x,z \le 200$ mm and $110 < y \le 200$ mm. Fig. 5(c), (d) and (e) are controlled using the same method. In the case of Fig. 5(e) with 100% mixing, the coordinates of all particles correspond to $0 \le x,y,z \le 200$ mm.

**Table 3**
Input parameters for the DEM simulation.

| Color | Material | Density [kg/m$^3$] | Number of particles | Diameter of particle [mm] |
|---|---|---|---|---|
| Purple | Beryllium | 1850 | 13,581 | 15 |
| Blue | Silicon | 2330 | 15,791 | 15 |
| Green | Aluminum | 2702 | 12,238 | 15 |
| Yellow | Aluminum alloy 2024-T6 | 2770 | 12,748 | 15 |
| Red | Aluminum alloy 195 | 2790 | 14,179 | 15 |

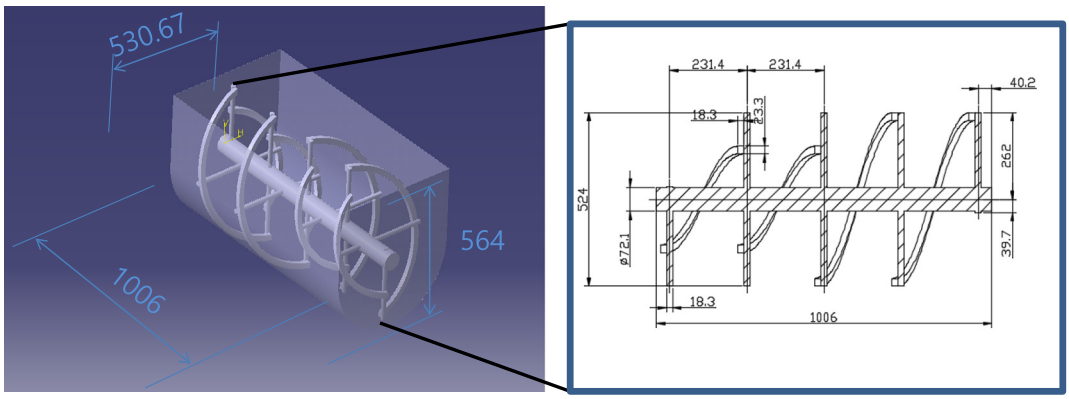


**Fig. 8.** Simplified canister geometry for DEM simulation of particle mixing. All dimensions are shown in mm.

The test domain was equally divided into 1000 subdomains ($10 \times 10 \times 10$). Fig. 6 shows the mixing indices for GMMI, MGMMI, and Lacey as well as for the proposed method (SMI). For the sampling method to compute the Lacey index, the equivalent particle number introduced in a study by Feng et al. [23] was used.

For the 0% mixing case, the SMI and Lacey index predicted no mixing, while the GMMI corresponded to 1.17 and 0.83 for particle types 1 and 2, respectively, and MGMMI corresponded to 0.83 for both types 1 and 2 particles. Fig. 6 also shows that all methods indicate a linear relationship between the mixing condition and mixing index. However, only the proposed index can predict the real mixing scenario beginning from a completely segregated case to a fully mixed case. The results in the case of the Lacey index are similar to those of the SMI although slightly higher values are displayed when compared to the SMI while indicating slightly different values during sampling. Both GMMI and MGMMI overestimated the mixing scenario for a low degree of mixing and this could potentially correspond to a reason for concern, specifically in the pharmaceutical industry. The computation time of the SMI exceeded those for the Lacey and MGMMI indices although it only lasted for a few seconds.

### 4.2. Model system for ternary mixing

We tested the index in a ternary system for a spherical domain. In this case, 4000 particles from each type of particles (green, red, and blue) were used and two different scenarios were considered. In the first case as shown in Fig. 7(a), the green particles are randomly distributed inside the inner most shell, the red particles are randomly distributed inside the middle shell and core, and the blue particles are randomly distributed inside all three shells. In the second case as shown in Fig. 7(b), the three types are completely separated in each shell.

Table 2 summarizes the mixing indices for the ternary system. The mixing index should be neither zero (fully separated) nor one (perfect mixing) in the case shown in Fig. 7(a). Conversely, a value of zero is expected for case 7(b) because each type of particle is completely separated. The proposed index corresponded to 0.3554 in case 7(a) and 0 in

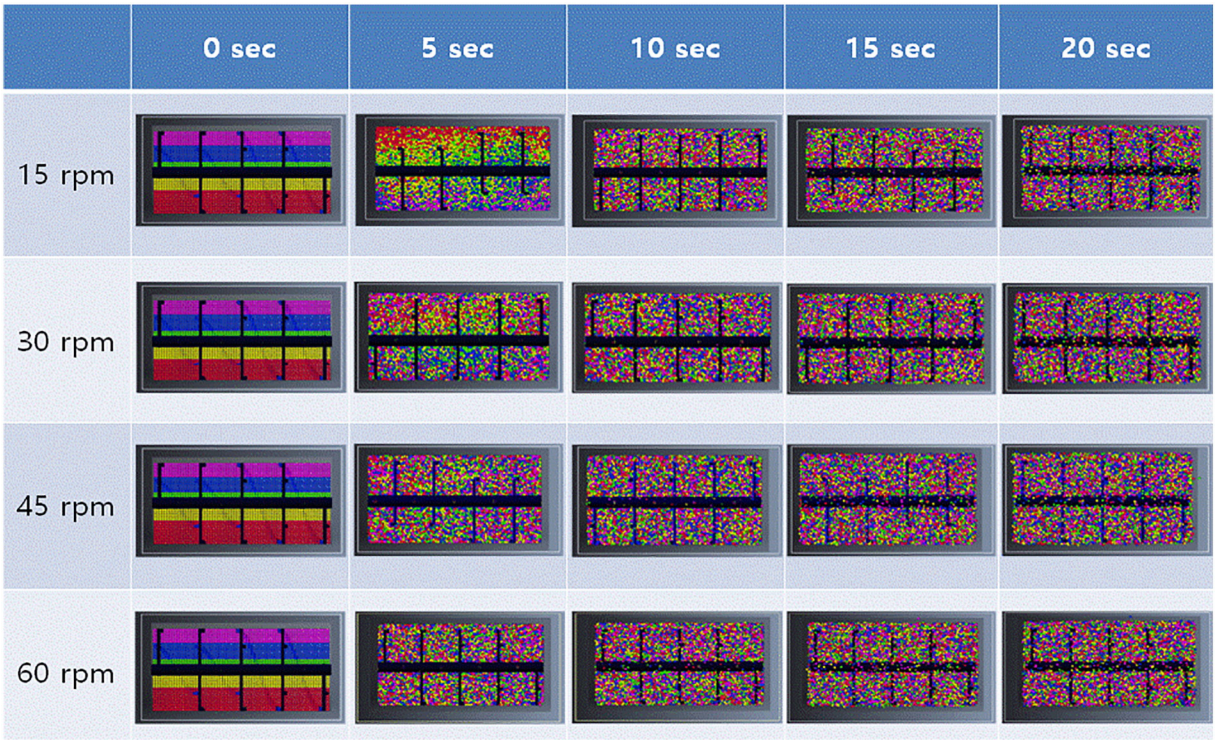


**Fig. 9.** Numerical simulation results of particle mixing at different times.

case 7(b). In contrast, both GMMI and MGMMI predicted nearly complete mixing in both cases. A major error in GMMI and MGMMI was due to the use of arbitrary mean values for the *x*, *y*, and *z* coordinates.

## 5. Study of particle mixing using discrete element method

Several computer simulation tools such as Monte Carlo simulations [33], molecular dynamics (MD) [34], Lattice Boltzmann method (LBM) [35], and the discrete element method (DEM) [36–39] were developed to study mixing. In the present study, DEM was used to study particle mixing in a screw blender. Specifically, DEM is useful to predict the motion of several small particles. It is similar to molecular dynamics (MD). However, DEM includes rotational degrees of freedom as well as close contact even in complex geometries.

Additionally, DEM tracks the motions and positions of individual particles with respect to time. The method was originally developed by Cundall and Strack to investigate soil behavior by using a 2D disc element [40]. The method is very important in various fields ranging from food and pharmaceuticals to agriculture and mining. The governing equations and numerical methods used in this method are briefly reviewed in the following section.

### 5.1. Equations of motion

The translational ($\vec{u}_i$) and rotational ($\vec{\omega}_i$) movements of particle *i* can be described as follows:

$$m_i \frac{d\vec{u}_i}{dt} = \sum_j \vec{F}_{c,ij} + m_i \vec{g} \tag{12}$$

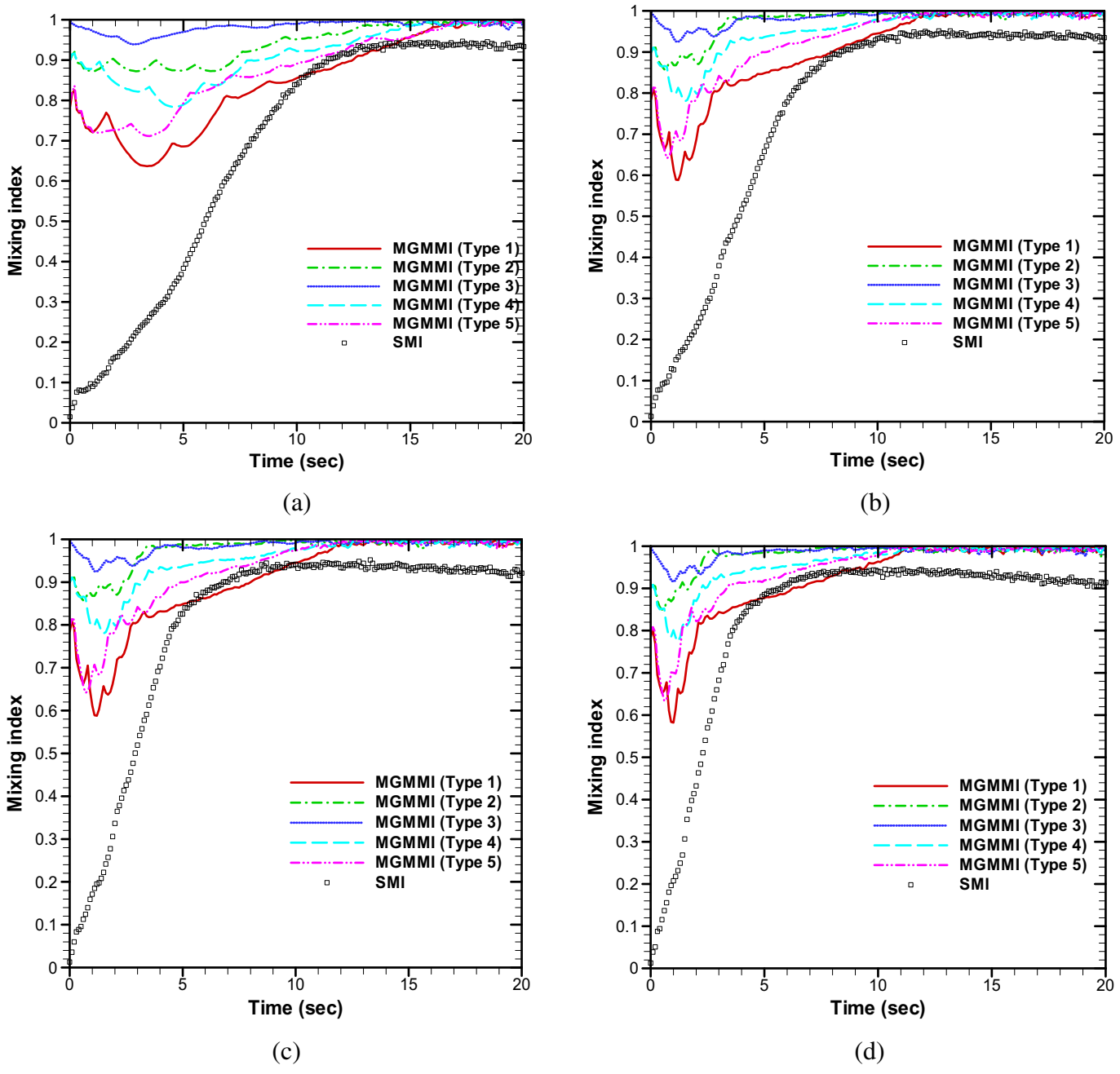


**Fig. 10.** Mixing indices for a multi-component mixture: (a) 15 rpm, (b) 30 rpm, (c) 45 rpm and (d) 60 rpm. Specifically, 125 subdomains are used to calculate the mixing index. The height of the subdomains is adjusted to obtain a completely segregated case at the beginning of the mixing process while uniform length and width are maintained.

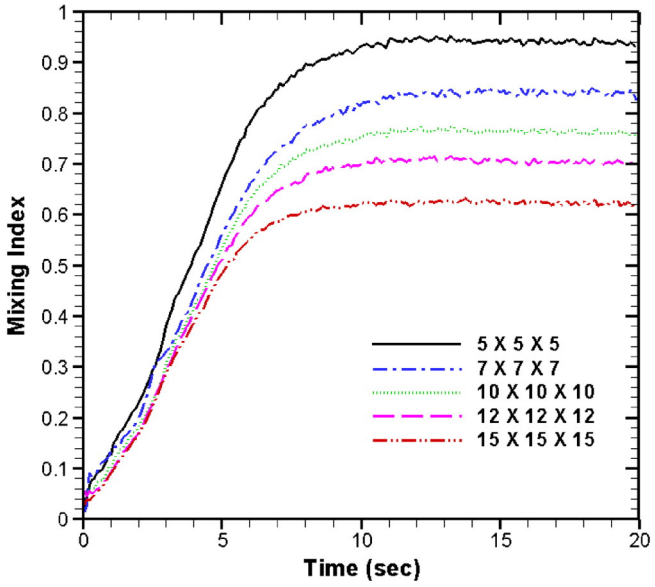


**Fig. 11.** Comparison of mixing indices with respect to the number of subdomains (30 rpm).

$$I_i \frac{d\vec{\omega}_i}{dt} = \sum_j \left( \vec{r}_{c,i} \times \vec{F}_{c,ij} + \vec{T}_{c,ij} \right) \quad (13)$$

where $m_i$ and $I_i$ denote the mass and moment of inertia, respectively, of particle $i$, $\vec{g}$ denotes gravitational acceleration, $\sum_j \vec{F}_{c,ij}$ denotes all forces acting on particle $i$ due to contact with other particles or the walls, and $\vec{r}_{c,i}$ denotes the distance between the center of particle $i$ and the other contact points. The terms on the right side of Eq. (13) correspond to external torques acting on the particle. A more detailed description of all forces on DEM model can be found in extant studies [37–39].

### 5.2. Numerical results of particle mixing in a screw blender

The mixing of five different types of spherical particles was simulated in a screw blender. The physical properties and numbers of each type are shown in Table 3. The total number of particles was maintained below 68,537 to ensure that the computational burden was at a reasonable level. Fig. 8 shows a schematic of the constant-pitch screw feeder used in the simulation. The particles are initially layered in a simplified canister geometry. A commercial software package (Particleworks, Prometech Software, Inc., Tokyo, Japan) was used to solve the equations of motion to determine the particle locations and velocities. Simulations were performed for four different rotation rates of the screw blender.

Fig. 9 shows the transient evolution of five-component mixtures at different rotation rates of the screw blender. Each type of particle was initially piled up layer by layer. The numerical results revealed that all types of particles were slightly mixed after rotation for 5 s. Subsequently, the degree of mixing qualitatively increased with increases in the rotation rate. However, after 10 s, it was hard to distinguish the degree of

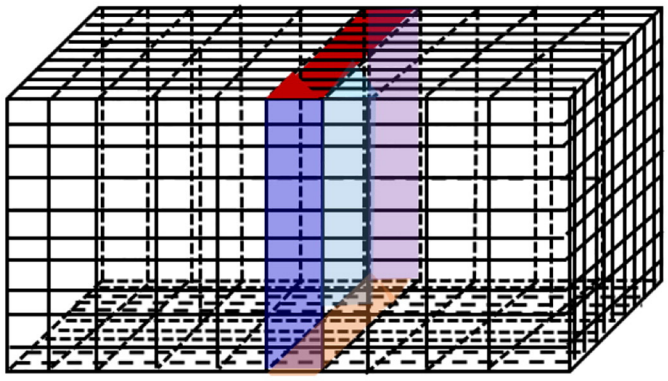

(a)

| | | | | | | | | | |
|---|---|---|---|---|---|---|---|---|---|
| 0 | 0 | 0 | 0 | 0 | 0 | 0 | 0 | 0 | 0 |
| 0 | 0.72 | 0.42 | 0.69 | 0.73 | 0.57 | 0.72 | 0.71 | 0.72 | 0 |
| 0 | 0.71 | 0.64 | 0.63 | 0.55 | 0.64 | 0.67 | 0.77 | 0.54 | 0 |
| 0 | 0.46 | 0.39 | 0.48 | 0.41 | 0.51 | 0.62 | 0.65 | 0.61 | 0 |
| 0 | 0.44 | 0.39 | 0.39 | 0.37 | 0.48 | 0.55 | 0.46 | 0.57 | 0 |
| 0 | 0.35 | 0.45 | 0.49 | 0.41 | 0.38 | 0.49 | 0.55 | 0.63 | 0 |
| 0 | 0.63 | 0.38 | 0.57 | 0.42 | 0.53 | 0.44 | 0.61 | 0.43 | 0 |
| 0 | 0.53 | 0.61 | 0.55 | 0.29 | 0.51 | 0.43 | 0.47 | 0.59 | 0 |
| 0 | 0.59 | 0.73 | 0.58 | 0.48 | 0.66 | 0.45 | 0.56 | 0.50 | 0 |
| 0 | 0.49 | 0.55 | 0.47 | 0.69 | 0.56 | 0.55 | 0.57 | 0.44 | 0 |

(b)

| | | | | | | | | | |
|---|---|---|---|---|---|---|---|---|---|
| 0 | 0 | 0.38 | 0 | 0 | 0 | 0 | 0 | 0 | 0 |
| 0 | 0.90 | 0.78 | 0.78 | 0.78 | 0.69 | 0.88 | 0.67 | 0.83 | 0 |
| 0 | 0.70 | 0.80 | 0.73 | 0.56 | 0.73 | 0.65 | 0.65 | 0.73 | 0 |
| 0 | 0.88 | 0.86 | 0.92 | 0.70 | 0.72 | 0.85 | 0.73 | 0.88 | 0 |
| 0 | 0.57 | 0.79 | 0.69 | 0.53 | 0.74 | 0.67 | 0.71 | 0.79 | 0 |
| 0 | 0.79 | 0.83 | 0.71 | 0.75 | 0.88 | 0.87 | 0.63 | 0.68 | 0 |
| 0 | 0.86 | 0.86 | 0.82 | 0.62 | 0.71 | 0.84 | 0.81 | 0.55 | 0 |
| 0 | 0.82 | 0.56 | 0.81 | 0.64 | 0.74 | 0.82 | 0.71 | 0.66 | 0 |
| 0 | 0.84 | 0.83 | 0.81 | 0.66 | 0.88 | 0.78 | 0.89 | 0.82 | 0 |
| 0 | 0.79 | 0.65 | 0.61 | 0.63 | 0.56 | 0.74 | 0.73 | 0.86 | 0 |

(c)

| | | | | | | | | | |
|---|---|---|---|---|---|---|---|---|---|
| 0 | 0.5 | 0.5 | 0.42 | 0.25 | 0.25 | 0.08 | 0.15 | 0.5 | 0 |
| 0.42 | 0.86 | 0.76 | 0.69 | 0.61 | 0.76 | 0.89 | 0.80 | 0.73 | 0.25 |
| 0.33 | 0.86 | 0.69 | 0.71 | 0.68 | 0.79 | 0.87 | 0.74 | 0.77 | 0.38 |
| 0.33 | 0.80 | 0.82 | 0.74 | 0.78 | 0.89 | 0.69 | 0.89 | 0.86 | 0.50 |
| 0.38 | 0.76 | 0.78 | 0.81 | 0.69 | 0.68 | 0.71 | 0.75 | 0.72 | 0.58 |
| 0.33 | 0.71 | 0.74 | 0.76 | 0.80 | 0.78 | 0.76 | 0.72 | 0.67 | 0.38 |
| 0.13 | 0.74 | 0.64 | 0.77 | 0.65 | 0.74 | 0.70 | 0.68 | 0.82 | 0.17 |
| 0.17 | 0.75 | 0.77 | 0.70 | 0.62 | 0.78 | 0.69 | 0.85 | 0.77 | 0.25 |
| 0.5 | 0.79 | 0.90 | 0.84 | 0.92 | 0.77 | 0.72 | 0.77 | 0.65 | 0.33 |
| 0.42 | 0.73 | 0.66 | 0.67 | 0.84 | 0.69 | 0.66 | 0.76 | 0.78 | 0.25 |

(d)

**Fig. 12.** Spatial distribution of mixing indices: (a) subdomains, (b) mixing index at $t = 5$ s, (c) mixing index at $t = 10$ s, and (d) mixing index at $t = 20$ s.

mixing with respect to the rotation rate. In order to compute SMI, 125 ($n_w = 5$, $n_h = 5$, $n_d = 5$) subdomains were created. Indices were also calculated using other methods for purposes of comparison.

Fig. 10(a)–(d) show a comparison of the mixing indices for MGMMI and SMI for a multi-component mixture. In this case, only MGMMI is considered for purposes of comparison because it corresponds to the modified GMMI and generally provides a better result when compared with the GMMI. The results for MGMMI for a multi-component mixture indicated that it converged to a value close to 1 after 17 s, 15 s, 12 s, and 11 s for 15 rpm, 30 rpm, 45 rpm, and 60 rpm, respectively. Nevertheless, the value of MGMMI was between 0.6 and 0.9 in a very early stage of the mixing process, which is unreasonable. In contrast, the SMI commenced with 0 and reached a maximum of 0.94. It was assumed that the equilibrium mixing phase was attained when there was no significant change in the SMI value. The mixing index indicated that it was possible to achieve equilibrium mixing states at 13 s, 11 s, 8.5 s, and 7.5 s for 15 rpm, 30 rpm, 45 rpm, and 60 rpm, respectively.

Fig. 10(a)–(d) also indicate that the value of the proposed index was slightly lower when compared with that of the MGMMI during the equilibrium state. In all cases, MGMMI reached 1, thereby indicating perfect mixing of all five components. Perfect mixing is highly unlikely in reality, and the most likely outcome of this mixing mechanism corresponds to a randomly mixed scenario as presented in Fig. 1(c). Moreover, the mixing index corresponded to about 0.90–0.94 although the particle distributions shown in this case resemble that in a well-mixed problem. This suggested that MGMMI over-predicted the mixing index for both the equilibrium and the initial mixing phases. Additionally, the numerical results also indicated that the mixing index could experience a slight decrease after reaching its highest value. With the exception of computational uncertainty, this can be attributed to the higher momentum applied to a particle surface at a faster rotational speed as this can disturb a particle's position more easily.

### 5.3. Subdomain size

In the study, the effect of the number of subdomains on mixing index was examined. As shown in Fig. 11, the mixing index decreased when the number of subdomains increased from 125($5 \times 5 \times 5$) to 3375($15 \times 15 \times 15$). The same DEM simulation was used for 30 rpm of the multi-mixture in Fig. 10(b). The minimum volume of a subdomain (the total volume of particles that are composed of single particles representing each type) corresponds to a criterion for the perfect mixing as shown in Fig. 1(d). The mixing index obtained from the small size of the subdomain implies the mixing index which is seen from the viewpoint of the perfect mixing condition of Fig. 1(d). However, a big size of the subdomain provides a mixing index value seen from the perspective of the fully random mixing condition of Fig. 1(c).

Information on spatial distribution of mixing states within a mixing device is useful for designing related parts that determine a mixing performance. In this study, the mixing states are examined by presenting the local SMI(i) within the computational domain during the mixing process. Fig. 12 shows a 2D spatial image of the mixing index in the computational domain. The number of subdomains corresponded to $10 \times 10 \times 10$ for rpm 30 as shown in Fig. 11. Fig. 12(b)–(d) are obtained from the near center of the computational domain as shown in Fig. 12(a). As shown in Fig. 12(b), the mixing indices were zero at the boundaries at 5 s. As shown in Fig. 12(c), one of the mixing indices corresponded to 0.38 at the upper boundary at 10 s. Finally, all the boundaries had none zero mixing values with the exception of the upper two corners as shown in Fig. 12(d). We found that mixing near walls was not good due to the wall effect.

Proper selection of the subdomains is key to the index. In order to accurately predict the mixing index, the face of a subdomain should be in line with the initial particle loading interface as an erroneous mixing index will be obtained otherwise. Another important factor corresponds to the size of the subdomain. For example, the mixing index will always correspond to one if a subdomain is considered for the whole system. In contrast, the subdivision mixing index (SMI) will approach zero if the subdomain is smaller than a particle. The proper size and shape of a subdomain depends on the problem geometry in a manner similar to any deterministic computational work including finite volume, difference or element methods. However, the subdomain size cannot be infinitely small as opposed to those in the forementioned predictive methods. The characteristic length of the subdomain should exceed the combined diameters of each type of particle.

## 6. Conclusions

We proposed a new non-sampling mixing index for multi-component mixtures and binary mixtures. The index was validated for a number of test cases. The results indicate that index can overcome several widely-known disadvantages of existing indices based on statistics and non-sampling methods. The proposed index includes several advantages. First, the SMI index corresponds to zero when the particle types are completely separated or segregated and corresponds to one when a mixture is perfectly mixed. Second, the values of the index range between 0 and 1 and linearly increase with increases in the degree of mixing. Third, SMI is computed in the same manner for both a binary mixture and a multi-component mixture. Fourth, in contrast to the MGMMI, SMI determines a single mixing index irrespective of whether binary or multi-component mixtures are used regardless of the number of components. Fifth, it is not necessary for the SMI to consider sampling methods, and thus it can overcome the limit of the mixing index based on statistics. Sixth, SMI can be computed within a few seconds because the number of each particle type to obtain SMI is counted. Thus, the findings reveal that SMI is a very good tool for evaluating mixing quality. The index value depends on the size of subdomains, and therefore the proper selection of subdomains is very important for the prediction. The index can also be applied in other research fields such as racial diversity estimation in an institute.

## Acknowledgments

This work was supported by a National Research Foundation (NRF) of Korea grant funded by the Government of Korea (MSIP) (No. 2015R1C1A2A01052256).

## References

[1] B. Remy, J.G. Khinast, B.J. Glasser, Discrete element simulation of free flowing grains in a four-bladed mixer, AIChE J. 55 (2009) 2035–2048.
[2] S.I. Badawy, T.J. Lee, M.M. Menning, Effect of drug substance particle size on the characteristics of granulation manufactured in a high-shear mixer, AAPS PharmSciTech 1 (2000) E33.
[3] R.K. Thakur, C. Vial, K.D.P. Nigam, E.B. Nauman, G. Djelveh, Static mixers in the process industries — a review, Chem. Eng. Res. Des. 81 (2003) 787–826.
[4] H. Hoornahad, E.A.B. Koenders, Towards simulation of fresh granular-cement paste material behavior, in: P.C. Wang, L. Ai, Y.G. Li, X.M. Sang, J.L. Bu (Eds.) Manufacturing Science and Technology, Pts 1-32011 pp. 2171–2177.
[5] J. Chen, L. Zeng, J. Yin, Discrete element method (DEM) analyses of hot-mix asphalt (HMA) mixtures compaction and internal structure, in: X.Y. Zhou, G.J. He, Y.L. Fan, Y. Xiao, S.K. Kunnath, G. Monti (Eds.),Advances in Civil Infrastructure Engineering, Pts 1 2013, pp. 1287–1294.
[6] A.H. Bloksma, Rheology of the breadmaking process, Cereal Foods World. 35 (1990) 228–236.
[7] R.K. Connelly, J.L. Kokini, Examination of the mixing ability of single and twin screw mixers using 2D finite element method simulation with particle tracking, J. Food Eng. 79 (2007) 956–969.
[8] P.M. Portillo, M.G. Ierapetritou, F.J. Muzzio, Characterization of continuous convective powder mixing processes, Powder Technol. 182 (2008) 368–378.
[9] J.N. Staniforth, J.E. Rees, Effect of vibration time, frequency and acceleration on drug content uniformity, J. Pharm. Pharmacol. 34 (1982) 700–706.
[10] B. Banfai, K. Ganzler, S. Kemeny, Content uniformity and assay requirements in current regulations, J. Chromatogr. A 1156 (2007) 206–212.
[11] M.K. Freeman, W. White, M. Iranikhah, Tablet splitting: a review of weight and content uniformity, Consult Pharm. 27 (2012) 341–352.
[12] N. Harnby, M.F. Edwards, A.W. Nienow, Mixing in the Process Industries, second ed Butterworth Heinemann, Oxford, UK, 1992.

[13] B. Laurent, J. Bridgwater, D. Parker, Motion in a particle bed agitated by a single blade, AICHE J. 46 (2000) 1723–1734.
[14] S. Corrsin, Simple theory of an idealized turbulent mixer, AICHE J. 3 (1957) 329–330.
[15] G. Basinskas, M. Sakai, Numerical study of the mixing efficiency of a ribbon mixer using the discrete element method, Powder Technol. 287 (2016) 380–394.
[16] F. Qi, T.J. Heindel, M.M. Wright, Numerical study of particle mixing in a lab-scale screw mixer using the discrete element method, Powder Technol. 308 (2017) 334–345.
[17] M. Alian, F. Ein-Mozaffari, S.R. Upreti, Analysis of the mixing of solid particles in a plowshare mixer via discrete element method (DEM), Powder Technol. 274 (2015) 77–87.
[18] D.E.M. Gooding, Quasi-Static Compression Forming of Stabilised Soil-Cement Building Blocks, Development Technology Unit, University of Warwick, Coventry, England, 1993.
[19] S. Wu, K. Zhang, H. Wen, J. Devol, K. Kelsey, Performance evaluation of hot mix asphalt containing recycled asphalt shingles in Washington State, J. Mater. Civ. Eng. 28 (2016).
[20] J.C. Williams, The mixing of dry powders, Powder Technol. 2 (1968) 13–20.
[21] P. Lacey, Developments in the theory of particle mixing, J. Appl. Chem. 4 (1954) 257–268.
[22] P. Lacey, The mixing of solid particles, Chem. Eng. Res. Des. 75 (1997) S49–S55.
[23] Y.Q. Feng, B.H. Xu, S.J. Zhang, A.B. Yu, P. Zulli, Discrete particle simulation of gas fluidization of particle mixtures, AICHE J. 50 (2004) 1713–1728.
[24] B.N. Asmar, P.A. Langston, A.J. Matchett, A generalised mixing index in distinct element method simulation of vibrated particulate beds, Granul. Matter 4 (2002) 129–138.
[25] M.S. Siraj, S. Radl, B.J. Glasser, J.G. Khinast, Effect of blade angle and particle size on powder mixing performance in a rectangular box, Powder Technol. 211 (2011) 100–113.
[26] G. Chandratilleke, A. Yu, J. Bridgwater, K. Shinohara, A particle-scale index in the quantification of mixing of particles, AICHE J. 58 (2012) 1099–1118.
[27] J. Butters, Recent developments in the mixing of dry solids, Br. Chem. Eng. 15 (1970) 41–43.
[28] R.G. Holdrich, Fundamentals of Particle Technology, Midland Information Technology and Publishing, Shepsted, Leceistershire, UK, 2002.
[29] L. Fan, Y.-M. Chen, F. Lai, Recent developments in solids mixing, Powder Technol. 61 (1990) 255–287.
[30] L. Fan, S. Chen, C. Watson, Annual review solids mixing, Ind. Eng. Chem. 62 (1970) 53–69.
[31] H.A. Kramer, Effect of grain velocity and flow rate upon the performance of a diverter type sampler, U. S. Department of Agriculture, Agricultural Research Service, ARS No. 51-25, 1968.
[32] M.D. Ashton, F.H.H. Valentin, The mixing of powders and particles in industrial mixers, Trans. Inst. Chem. Eng. 44 (5) (1966) 166–188.
[33] C.R.A. Abreu, F.W. Tavares, M. Castier, Influence of particle shape on the packing and on the segregation of spherocylinders via Monte Carlo simulations, Powder Technol. 134 (2003) 167–180.
[34] D.C. Hong, J.A. McLennan, Molecular-dynamics simulations of hard-sphere granular particles, Physica A 187 (1992) 159–171.
[35] H.B. Li, H.P. Fang, Z.F. Lin, S.X. Xu, S.Y. Chen, Lattice Boltzmann simulation on particle suspensions in a two-dimensional symmetric stenotic artery, Phys. Rev. E 69 (2004).
[36] L. Vu-Quoc, X. Zhang, O.R. Walton, A 3-D discrete-element method for dry granular flows of ellipsoidal particles, Comput. Methods Appl. Mech. Eng. 187 (2000) 483–528.
[37] S. Luding, Introduction to discrete element methods: basic of contact force models and how to perform the micro-macro transition to continuum theory, Eur. J. Environ. Civ. Eng. 12 (2008) 785–826.
[38] Y. Tan, R. Deng, Y.T. Feng, H. Zhang, S. Jiang, Numerical study of concrete mixing transport process and mixing mechanism of truck mixer, Eng. Comput. 32 (2015) 1041–1065.
[39] R. Deng, Y. Tan, H. Zhang, X. Xiao, S. Jiang, Experimental and DEM studies on the transition of axial segregation in a truck mixer, Powder Technol. 314 (2017) 148–163.
[40] P.A. Cundall, O.D.L. Strack, A discrete numerical model for granular assemblies, Geotechnique 29 (1979) 47–65.